

Supplementary Material

Altered global brain network topology as a trait marker in patients with anorexia nervosa

Daniel Geisler MSc,¹ Viola Borchardt PhD,^{2,3} Ilka Böhm PhD,¹ Joseph A. King PhD,¹
Friederike I. Tam MD,^{1,4} Michael Marxen PhD,⁵ Ronald Biemann PhD,⁶ Veit Roessner MD,⁴
Martin Walter MD,^{2,3,7,8} Stefan Ehrlich MD^{*,1,4}

- ¹ Division of Psychological and Social Medicine and Developmental Neuroscience, Faculty of Medicine, Technische Universität Dresden, Dresden, Germany
- ² Clinical Affective Neuroimaging Laboratory, Magdeburg, Germany
- ³ Department of Behavioral Neurology, Leibniz Institute for Neurobiology, Magdeburg, Germany
- ⁴ Eating Disorder Treatment and Research Center, Department of Child and Adolescent Psychiatry, Faculty of Medicine, Technische Universität Dresden, Dresden, Germany
- ⁵ Department of Psychiatry and Neuroimaging Center, Technische Universität Dresden, Dresden, Germany
- ⁶ Institute of Clinical Chemistry and Pathobiochemistry, Otto-von-Guericke University, Magdeburg, Germany
- ⁷ Clinic for Psychiatry and Psychotherapy, Eberhard-Karls University, Tuebingen, Germany
- ⁸ Center for Behavioral Brain Sciences (CBBS), Magdeburg, Germany

1 Methods

1.1 Participants and assessments

HCs were recruited through advertisement among middle school, high school and university students. For case-control age-matching, an implementation of the Munkres algorithm (Munkres 1957) was used. The matching procedure resulted in a maximum difference of 0.6 years between the individuals within one recAN-HC pair (mean age difference of 0.2 years).

Exclusion criteria and possible confounding variables, e.g. the use of psychotropic medications and medical comorbidities, were obtained using the SIAB-EX and our own semi-structured interview. Comorbid psychiatric diagnoses other than eating disorders were derived from medical records and confirmed by an expert clinician with over 10 years of experience after careful chart review (including consideration of medical and psychiatric history and a range of psychiatric screening instruments).

HC participants were excluded if they had any history of psychiatric illness, a lifetime BMI below the 10th age percentile if younger than 18 years or a BMI below 18.5kg/m² if older than 18 years, or were currently obese (BMI over 92th age percentile if younger than 18 years; BMI over 29kg/m² if older than 18 years).

Participants of both study groups were excluded if they had a lifetime history of any of the following clinical diagnoses: organic brain syndrome, schizophrenia, substance dependence, psychosis NOS, bipolar disorder, bulimia nervosa or binge-eating disorder (or “regular” binge eating - defined as bingeing at least once a week for 3 or more consecutive months). Further exclusion criteria for all participants were IQ lower than 85; psychotropic medication (other than SSRI) within 4 weeks prior to the study; current substance abuse; current inflammatory, neurologic or metabolic illness; chronic medical or neurological illness that could affect appetite, eating behavior, or body weight (e.g., diabetes); clinically relevant anemia; pregnancy; and breast feeding.

In recAN, comorbid diagnoses were taken according to standard practice from medical records and confirmed by an expert clinician with over 10 years of experience after careful chart review (including consideration of medical and psychiatric history and a range of psychiatric screening instruments e.g. SIAB-EX, EDI-2, BDI-2, SCL-90-R, see Table S1). 23% of the recAN participants had a history of one or more formal comorbid psychiatric diagnoses (22% depressive disorders including dysthymia, 1% obsessive-compulsive disorder, and 4% anxiety disorder).

All recAN subjects had a BMI in the past below the cut-offs defining AN according to Kromeyer-Hauschild et al. (2001) and Hebebrand et al. (2004).

Handedness was assessed using a short version of the Annett Scale of Hand Preference (Annett 1970) as previously implemented in Gollub et al. (2013). This questionnaire asks for handedness in typical daily life situations as writing or brushing teeth. Response categories range from 0 'right hand', 1 'both hands' to 2 'left hand'. A mean score for handedness was calculated. For a list of other employed assessment instruments see Table S1.

Study data were collected and managed using secure, web-based electronic data capture tools REDCap (Research Electronic Data Capture (Harris *et al.* 2009)).

1.2 Laboratory measures

To measure leptin levels, venous blood was collected into vacutainer tubes between 7 and 9 a.m. after overnight fasting. Plasma samples were centrifuged (2500g for 15 min), aliquoted, and stored at -80°C until analysis. Hormone concentration in all participants was measured in one session at the same lab using a commercially available sandwich Enzyme Linked-Immunosorbent Assay (ELISA; BioVendor) following manufacturer instructions.

Inventory	Abbreviation	Description	Reference
Structured Interview for Anorexia and Bulimia Nervosa for DSM-IV	SIAB-EX	expert interview	(Fichter & Quadflieg 2001)
Beck Depression Inventory 2	BDI-2	self-report	(Hautzinger <i>et al.</i> 2009)
Eating Disorder Inventory 2	EDI-2	self-report	(Paul & Thiel 2005)
Revised symptom checklist 90	SCL-90-R	self-report	(Schmitz <i>et al.</i> 2000)
Wechsler Adult Intelligence Scale (short version)	WAIS	standardized assessment	(von Aster <i>et al.</i> 2006)
Wechsler Intelligence Scale for Children (short version)	WISC	standardized assessment	(Petermann & Petermann 2006)

Table S1. Assessment instruments. Intelligence quotient (IQ) was assessed with WAIS for participants aged ≥ 16 years or WISC otherwise.

1.3 MRI data acquisition

The T1-weighted structural brain scans were acquired with rapid acquisition gradient echo (MP-RAGE) sequence: number of slices=176; TR=1900ms; TE=2.26ms; flip angle=9°; slice thickness=1mm; voxel size=1x1x1mm³; FoV=256x224mm²; bandwidth=200 Hz/pixel.

1.4 MRI data processing & computation of graph metrics

Beyond SPM8 (<http://www.fil.ion.ucl.ac.uk/spm/>), the following software tools were used: DARTEL (Ashburner 2007) for generating anatomical group templates, Nipype framework (Gorgolewski *et al.* 2011) for running image processing workflows, DPARSFA toolbox (Yan & Zang 2010) for extraction of time series, open-source python library networkx (Hagberg *et al.* 2008) for graph analysis, and R toolbox (R Core Team 2012) for statistical analysis.

We evaluated the quality of the fMRI data by visual inspection. During preprocessing smoothing was not performed, because it would impose new correlations amongst seed regions, emphasizing those that are adjacent and hence bias the network structure towards a lattice topology

and alter graph metrics (Fornito *et al.* 2010). Similarly, during preprocessing we did not apply global mean regression, which would bias correlations and complicates the interpretation of negative correlations (Saad *et al.* 2012). There was no difference in global signal between groups ($t(100)=-0.89, p=0.38$).

A component based method (CompCor) was applied to the data in order to reduce signals that are unlikely to be modulated by neural activity (Behzadi *et al.* 2007).

To reduce the bias of residual motion through causing spurious correlation structures throughout the brain, which would be reflected in the derived graph metrics, the datasets were scrubbed after regression of nuisance covariates to eliminate timepoints with a framewise displacement $>0.5\text{mm}$ (Power *et al.* 2012). According to standard procedure of scrubbing, one preceding and two subsequent timepoints were also excluded (Power *et al.* 2012). A two-sample t-test was used to test for potential differences of frame-wise displacement and subsequently for differences in length of time series after scrubbing. Groups did not differ in the number of scrubbed frames ($\text{Mean}_{\text{HC}}=17.2, \text{SD}_{\text{HC}}=19.7; \text{Mean}_{\text{recAN}}=14.8, \text{SD}_{\text{recAN}}=18.1; t(107.3)=-0.66, p=0.51$) and none of the participants had less than 118 (equivalent to $>60\%$) frames after scrubbing. Therefore, no participant had to be excluded.

Preprocessed volumes were parcellated into 160 spherical regions of interest (ROIs) as defined by Dosenbach (2010). This functionally defined parcellation scheme has been derived from meta-analyses of task-related fMRI studies, covers cerebrum and cerebellum and consists of non-overlapping spheres with a diameter of 10mm. See Table S2 for a comprehensive list of all ROIs and the coordinates. The symmetric matrix of Pearson correlations provided the basis for graph generation.

The graphs were rendered sparse by recursively removing edges, beginning with the weakest weights and progressing until a certain percentage of edges remained. In order to investigate the influence of different sparsity threshold levels on network properties, 21 sparsity thresholds were

tested, starting from 10% in increasing steps of 1% to 30%. If removal of an edge would result in a disconnected graph, the respective edge was retained, even in case of low weight.

1.5 Local graph metrics

The degree of a node is the most basic local network measure and equals the number of the node's adjacent edges. A node with a high degree is densely connected and thus has a high importance in the network. The strength of a node is the sum of weights of edges from neighboring nodes connected to the node. A node with a high strength has a high temporal correlation with its neighboring nodes. The local clustering coefficient (CC_{loc}) is the ratio of triangles around the node meaning the fraction between the number of existing edges within the neighborhood of the node and the number of possible edges within the neighborhood of the node. CC_{loc} is used to measure segregation, which is the ability for specialized processing in small groups of nodes. A high CC_{loc} describes a node that is deeply embedded in a local subnetwork. The local characteristic pathlength (CPL_{loc}) is the number of edges in the shortest paths to any other node in the graph, normalized by the total number of nodes. As a measure of functional integration, a short CPL_{loc} reflects a rapid communication with distant brain regions. Betweenness centrality index (BCI) is the fraction of all shortest paths in the network that contain a given node. Nodes with a high BCI participate in a large number of shortest paths and are termed hubs. E_{loc} is the local efficiency computed on node neighborhoods describing extent of information transfer of the respective node with all other nodes in the network. A high E_{loc} expresses fast local flow of information. Normalized local efficiency ($LEGE$) equals E_{loc} after normalization based on global efficiency. The participation index (PI) is a measure of the diversity of intermodular connections of a given node.

1.6 Global graph metrics

The clustering coefficient (CC_{glob}) measures segregation and reflects the average diffusiveness of clustered connectivity around individual nodes. The characteristic pathlength (CPL_{glob}) between each possible pair of nodes is the number of edges in the shortest path between them, divided by all

possible pairs of nodes in the network. It measures the extent of overall routing efficiency, where a high CPL_{glob} represents less efficient information flow due to long routes. The ratio between clustering coefficient and characteristic pathlength after both metrics have been standardized by dividing their values by those of random networks preserving the degree distribution of the original graph is called small-world index (σ) and summarizes to what extent the network shows features of a small-world network. Small-world networks combine high local clustering with short paths, representing an effective system in which nodes are linked through relatively few edges. The global efficiency (E_{glob}) is the average inverse shortest pathlength and captures the extent of information propagation in the network. The assortativity (α) reflects the tendency of nodes wiring with nodes of similar degree. If nodes with similar (dissimilar) degree tend to wire together, the network is said to be assortative (disassortative). Networks with a positive assortativity are likely to have a comparatively resilient core of mutually interconnected high-degree nodes (Newman 2002; Hagmann *et al.* 2008). In contrast, networks with a negative assortativity are likely to have widely distributed and sparsely interconnected hubs. Biological networks show the property that nodes having high degrees are preferably connected with nodes having low degrees, i.e. disassortivity. On the contrary, social networks show the property that nodes having many connections tend to be connected with other highly connected nodes, i.e. assortativity.

To control for putative differences in overall connection strength, CC_{glob} and CPL_{glob} were normalized to 100 reference random graphs. All random graphs were connected and preserve degree distribution of the real graph.

1.7 Additional statistical analyses

Demographic and symptom variables were compared using Student's t-tests. Correlational analyses were performed using Pearson coefficients. In all statistical analyses we used age-adjusted BMI standard deviation scores (BMI-SDS) calculated using the LMS method from Cole (1990) and German population reference data from Kromeyer-Hauschild *et al.* (2001) for participants ≤ 18 years old and Hemmelmann *et al.* (2010) for participants ≥ 19 years old. BMI-SDS is a better measure than

absolute BMI in pediatric populations since what is considered a normal BMI changes with age (Hebebrand *et al.* 1996; Kromeyer-Hauschild *et al.* 2001).

1.8 Comparison with acute AN patients

As an exploratory analysis, the global metric assortativity of recAN was compared to the data of 35 acute patients from our previous study (Geisler *et al.* 2016). For better comparability, we recalculated assortativity from existing symmetric correlation matrices using the graph calculation procedure of the current study. Between-group comparisons were performed using non-parametric independent two-group Mann-Whitney U-Tests. We did not account for age differences.

ROI identifier	x	y	z	ROI identifier	x	y	z	ROI identifier	x	y	z
vmPFC_R_1	6	64	3	midinsula_R_55	33	-12	16	latcerebellum_L_109	-24	-54	-21
aPFC_R_2	29	57	18	midinsula_L_56	-36	-12	15	infcerebellum_L_110	-37	-54	-37
aPFC_L_3	-29	57	10	thalamus_L_57	-12	-12	6	postcingulate_R_111	10	-55	17
mPFC_4	0	51	32	thalamus_R_58	11	-12	6	precuneus_L_112	-6	-56	29
aPFC_L_5	-25	51	27	midinsula_R_59	32	-12	2	latcerebellum_L_113	-34	-57	-24
vmPFC_R_6	9	51	16	temporal_R_60	59	-13	8	IPS_L_114	-32	-58	46
vmPFC_L_7	-6	50	-1	midinsula_L_61	-30	-14	1	postcingulate_L_115	-11	-58	17
aPFC_R_8	27	49	26	parietal_L_62	-38	-15	59	IPS_R_116	32	-59	41
ventaPFC_R_9	42	48	-3	inftemporal_R_63	52	-15	-13	angulargyrus_R_117	51	-59	34
ventaPFC_L_10	-43	47	2	parietal_L_64	-47	-18	50	occipital_L_118	-34	-60	-5
vmPFC_L_11	-11	45	17	parietal_R_65	46	-20	45	occipital_R_119	36	-60	-8
vlPFC_R_12	39	42	16	parietal_L_66	-55	-22	38	medcerebellum_L_120	-6	-60	-15
vmPFC_R_13	8	42	-5	precentralgyrus_L_67	-54	-22	22	infcerebellum_L_121	-25	-60	-34
ACC_R_14	9	39	20	temporal_L_68	-54	-22	9	infcerebellum_R_122	32	-61	-31
vIPFC_R_15	46	39	-15	parietal_R_69	41	-23	55	temporal_R_123	46	-62	5
dIPFC_R_16	40	36	29	postinsula_R_70	42	-24	17	angulargyrus_L_124	-48	-63	35
supfrontal_R_17	23	33	47	basalganglia_R_71	11	-24	2	TPJ_L_125	-52	-63	15
vPFC_R_18	34	32	7	inftemporal_L_72	-59	-25	-15	occipital_L_126	-44	-63	-7
ACC_L_19	-2	30	27	postcingulate_R_73	1	-26	31	medcerebellum_L_127	-16	-64	-21
supfrontal_L_20	-16	29	54	parietal_R_74	18	-27	62	latcerebellum_R_128	21	-64	-22
ACC_L_21	-1	28	40	parietal_L_75	-38	-27	60	occipital_R_129	19	-66	-1
dIPFC_R_22	46	28	31	postinsula_L_76	-30	-28	9	medcerebellum_R_130	1	-66	-24
vPFC_L_23	-52	28	17	parietal_L_77	-24	-30	64	infcerebellum_L_131	-34	-67	-29
dIPFC_L_24	-44	27	33	temporal_R_78	51	-30	5	precuneus_R_132	11	-68	42
vFC_R_25	51	23	8	postparietal_L_79	-41	-31	48	occipital_R_133	17	-68	20
antinsula_R_26	38	21	-1	postcingulate_L_80	-4	-31	-4	IPS_L_134	-36	-69	40
dACC_R_27	9	20	34	fusiform_R_81	54	-31	-18	occipital_R_135	39	-71	13
antinsula_L_28	-36	18	2	temporal_L_82	-41	-37	16	occipital_L_136	-9	-72	41
dFC_R_29	40	17	40	temporal_L_83	-53	-37	13	occipital_R_137	45	-72	29
basalganglia_L_30	-6	17	34	fusiform_R_84	28	-37	-15	medcerebellum_L_138	-11	-72	-14
mFC_31	0	15	45	precuneus_L_85	-3	-38	45	occipital_R_139	29	-73	29
frontal_R_32	58	11	14	supparietal_R_86	34	-39	65	infcerebellum_R_140	33	-73	-30
vFC_L_33	-46	10	14	precuneus_R_87	8	-40	50	occipital_L_141	-2	-75	32
dFC_R_34	44	8	34	IPL_L_88	-41	-40	42	occipital_L_142	-29	-75	28
dFC_R_35	60	8	34	parietal_R_89	58	-41	20	medcerebellum_R_143	5	-75	-11
dFC_L_36	-42	7	36	postcingulate_L_90	-8	-41	3	medcerebellum_R_144	14	-75	-21
vFC_L_37	-55	7	23	inftemporal_L_91	-61	-41	-2	occipital_L_145	-16	-76	33
basalganglia_L_38	-20	6	7	occipital_L_92	-28	-42	-11	occipital_L_146	-42	-76	26
basalganglia_R_39	14	6	7	postcingulate_L_93	-5	-43	25	occipital_R_147	9	-76	14
vFC_L_40	-48	6	1	precuneus_R_94	9	-43	25	occipital_R_148	15	-77	32
pre-SMA_R_41	10	5	51	temporal_R_95	43	-43	8	occipital_R_149	20	-78	-2
vFC_R_42	43	1	12	IPL_R_96	54	-44	43	infcerebellum_L_150	-21	-79	-33
SMA_43	0	-1	52	parietal_L_97	-55	-44	30	infcerebellum_L_151	-6	-79	-33
midinsula_R_44	37	-2	-3	latcerebellum_L_98	-28	-44	-25	postoccipital_L_152	-5	-80	9
frontal_R_45	53	-3	32	postparietal_L_99	-35	-46	48	postoccipital_R_153	29	-81	14
precentralgyrus_R_46	58	-3	17	suptemporal_R_100	42	-46	21	postoccipital_R_154	33	-81	-2
thalamus_L_47	-12	-3	13	IPL_L_101	-48	-47	49	infcerebellum_R_155	18	-81	-33
midinsula_L_48	-42	-3	11	angulargyrus_L_102	-41	-47	29	postoccipital_L_156	-37	-83	-2
precentralgyrus_L_49	-44	-6	49	temporal_L_103	-59	-47	11	postoccipital_L_157	-29	-88	8
parietal_L_50	-26	-8	54	IPL_L_104	-53	-50	39	postoccipital_R_158	13	-91	2
precentralgyrus_R_51	46	-8	24	precuneus_R_105	5	-50	33	postoccipital_R_159	27	-91	2
precentralgyrus_L_52	-54	-9	23	occipital_L_106	-18	-50	1	postoccipital_L_160	-4	-94	12
precentralgyrus_R_53	44	-11	38	IPL_R_107	44	-52	47				
parietal_L_54	-47	-12	36	postcingulate_L_108	-5	-52	17				

Table S2. List of ROIs used for brain parcellation. Anatomical labels and MNI center coordinates are given as defined by Dosenbach (2010).

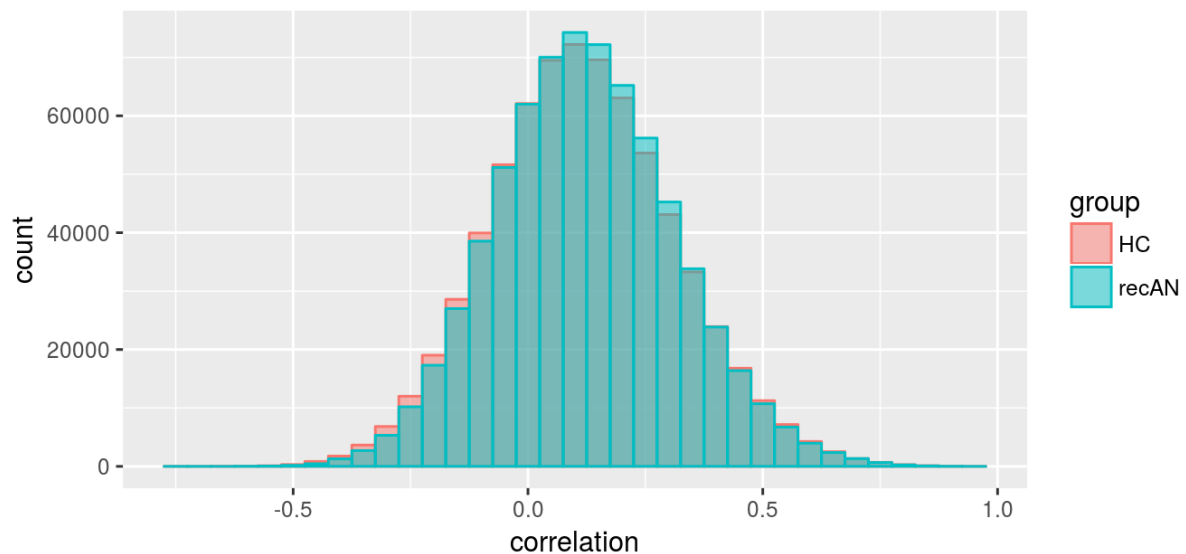


Figure S1. Distribution of correlations. Histogram of all Pearson correlation coefficients (values from the correlation matrices used for graph network construction) across groups. Recovered AN (recAN) and healthy controls (HC) are depicted by cyan and red, respectively.

2 Results

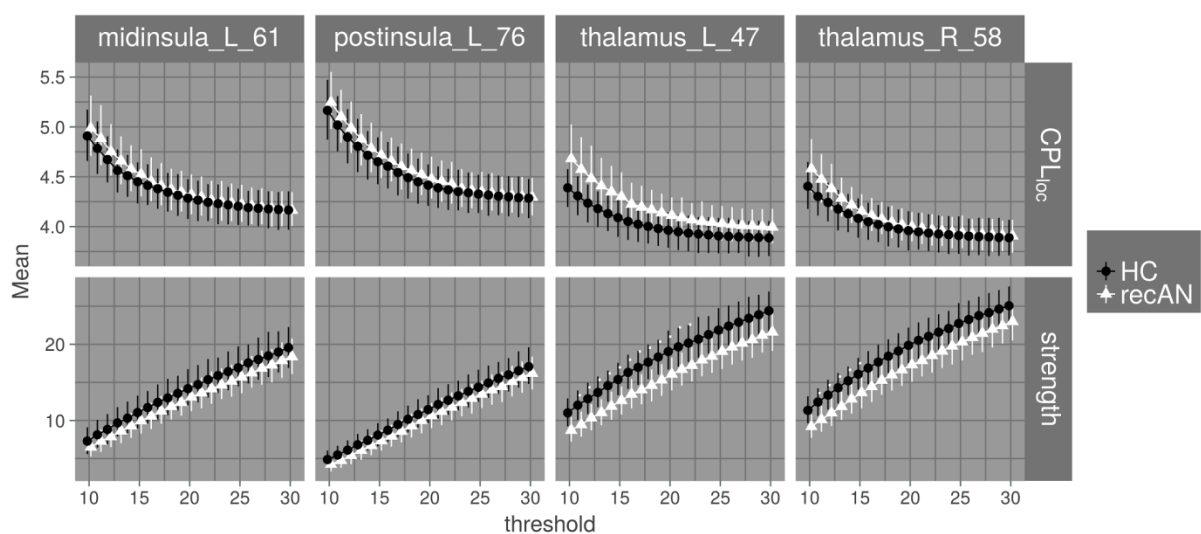


Figure S2. Group comparison of a priori selected local metrics. Results of group comparison of the two metrics local characteristic pathlength (CPL_{loc}) and strength of left midinsula, left postinsula, left and right thalamus for all tested sparsity thresholds between 10 and 30. Comparisons were done using Mann-Whitney U-Tests (** $p < 0.01$; * $p < 0.05$; · $p < 0.1$). According to our a priori hypothesis, p-values for CPL_{loc} and strength were not corrected for multiple comparisons. HC and recAN are depicted by black circles and white triangles, respectively.

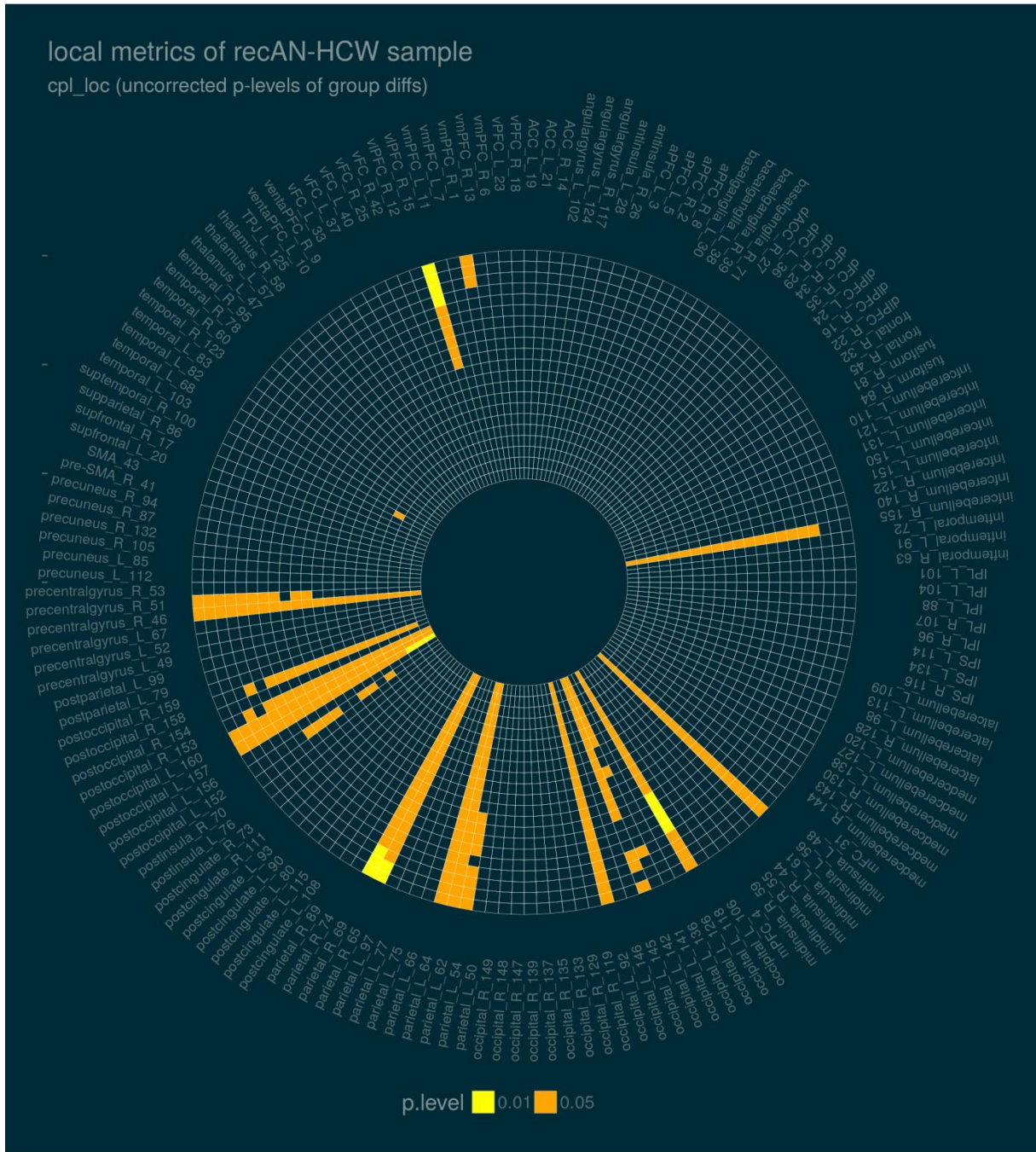


Figure S5. Group differences in local metrics - CPL_{loc}. Uncorrected significance levels of group comparisons for all ROIs and all tested sparsity thresholds are shown (least sparse in the center). None of these findings remained significant after correcting for multiple testing across regions and metrics.

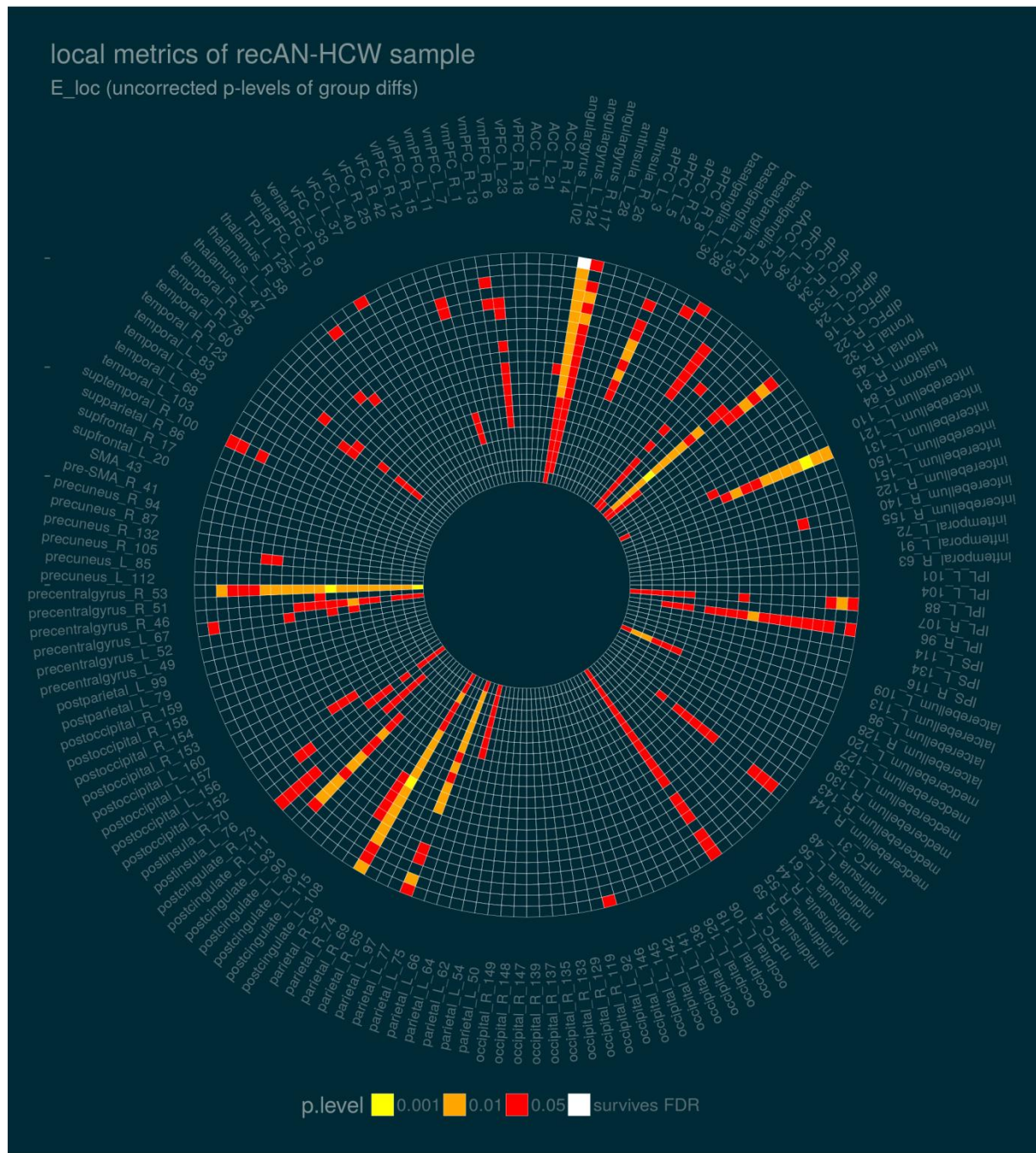


Figure S6. Group differences in local metrics - E_{loc} . Uncorrected significance levels of group comparisons for all ROIs and all tested sparsity thresholds are shown (least sparse in the center). Test statistics surviving correction for multiple testing of the 160 ROIs are highlighted in white. Please note that the latter FDR procedure did not take into account the number of tested local metrics (as described in the main manuscript). None of these findings remained significant after correcting for multiple testing across regions and metrics.

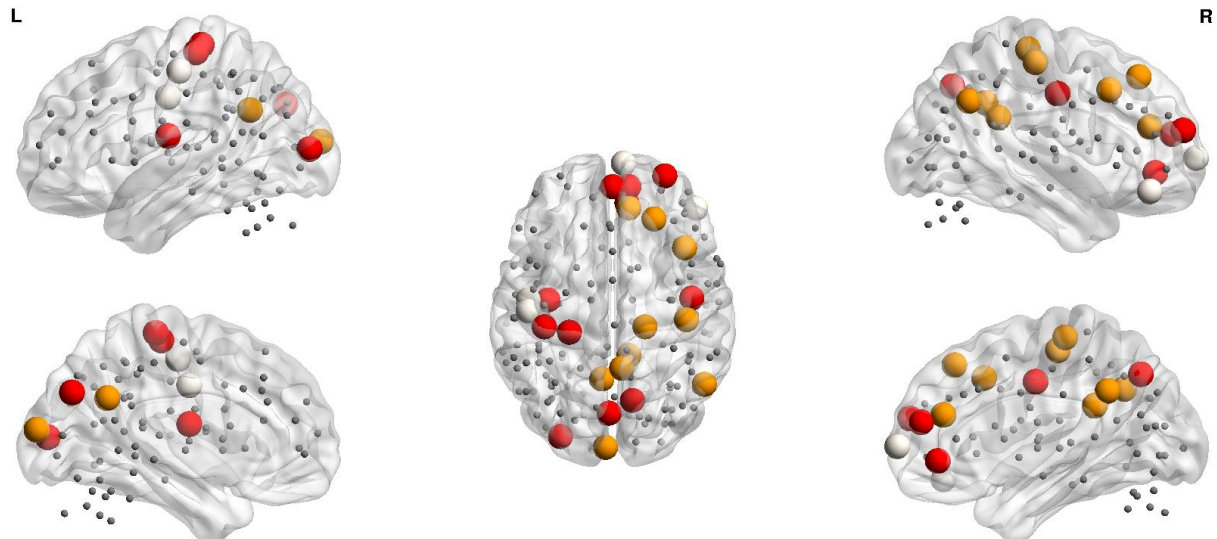


Figure S11. Localization of group differences in local metrics - Degree. Uncorrected significance levels of group comparisons for a sparsity thresholds of 10% are shown (yellow $p < 0.001$; orange $p < 0.01$; red $p < 0.05$). Nodes surviving correction for multiple testing of the 160 ROIs are highlighted in white. Please note that the latter FDR procedure did not take into account the number of tested local metrics (as described in the main manuscript). None of these findings remained significant after correcting for multiple testing across regions and metrics.

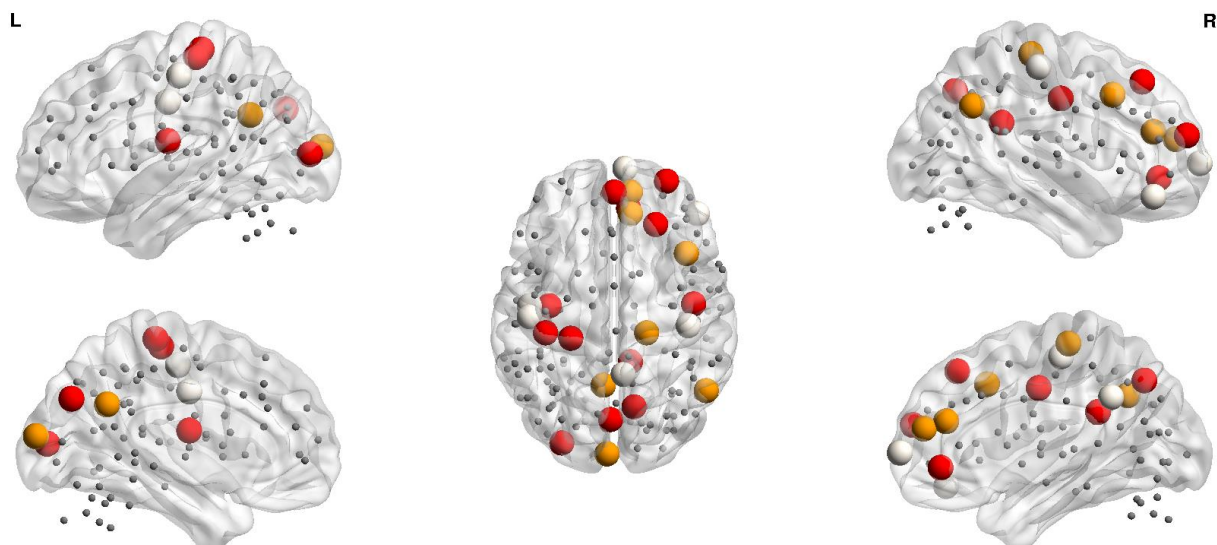


Figure S12. Localization of group differences in local metrics - Strength. Uncorrected significance levels of group comparisons for a sparsity thresholds of 10% are shown (yellow $p < 0.001$; orange $p < 0.01$; red $p < 0.05$). Node surviving correction for multiple testing of the 160 ROIs are highlighted in white. Please note that the latter FDR procedure did not take into account the number of tested local metrics (as described in the main manuscript). None of these findings remained significant after correcting for multiple testing across regions and metrics.

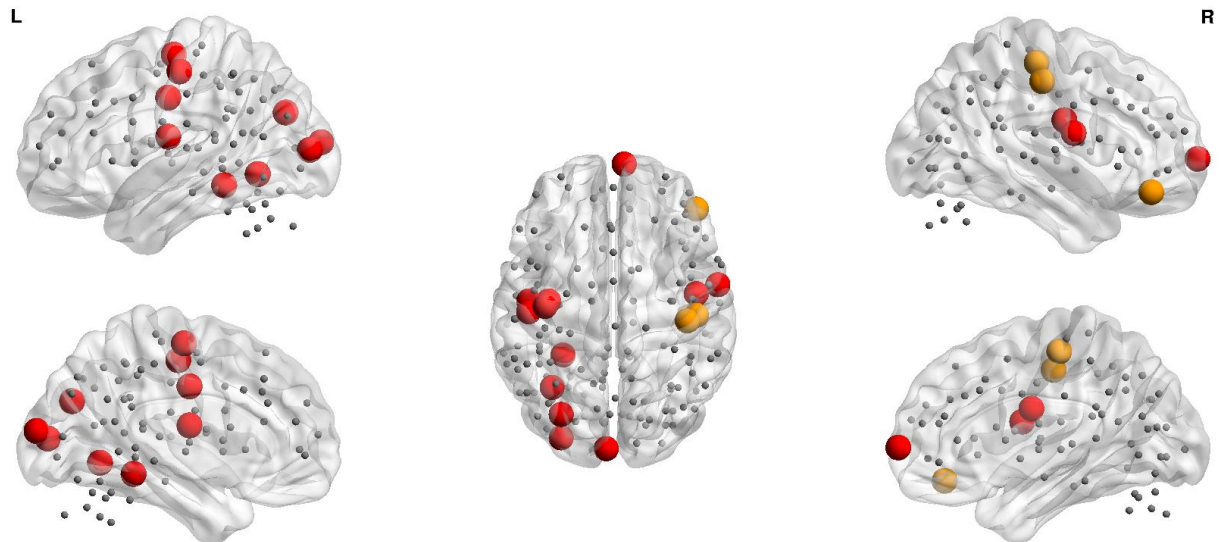


Figure S13. Localization of group differences in local metrics - CPL_{loc} . Uncorrected significance levels of group comparisons for a sparsity thresholds of 10% are shown (yellow $p < 0.001$; orange $p < 0.01$; red $p < 0.05$). None of these findings remained significant after correcting for multiple testing across regions and metrics.

ROI	Increase in recAN	p_{unc}
postoccipital_L_160	0.00137	0.0021
parietal_R_69	0.00129	0.0012
parietal_L_62	0.00116	0.0076
parietal_L_64	0.00105	0.0011
occipital_L_142	0.00103	0.0035
parietal_L_54	0.00101	0.0062
precentralgyrus_R_53	0.001	0.0066
parietal_R_74	0.001	0.0059
parietal_R_65	0.00072	0.0064

Table S3. Local assortativity. Brain regions showing increased local assortativity in recAN when compared to HC (uncorrected findings $p_{unc} < 0.01$). The values in this table reflect the AUC values of the metric *local assortativity* across all tested sparsity thresholds and all ROIs. After correcting the level of significance for the number of tested brain regions and metrics using FDR following the same approach as for other local graph metrics in our original manuscript, only the vIPFC_R_15 showed a trend for decreased local assortativity ($W=2159$, $p_{FDR}=0.064$). However, the average local assortativity across all 160 regions was significantly increased in recAN ($W=1100$, $p=0.02$). Thus, the increased global assortativity in recAN might be driven by multiple changes in local assortativity in several regions that do not reach significance.

3 References

- Annett M** (1970). A Classification of Hand Preference by Association Analysis. *British Journal of Psychology* **61**, 303–321.
- Ashburner J** (2007). A fast diffeomorphic image registration algorithm. *NeuroImage* **38**, 95–113.
- von Aster M, Neubauer AC, Horn R** (2006). *WIE - Wechsler Intelligenztest für Erwachsene*. Huber: Bern.
- Behzadi Y, Restom K, Liu J, Liu TT** (2007). A component based noise correction method (CompCor) for BOLD and perfusion based fMRI. *NeuroImage* **37**, 90–101.
- Cole TJ** (1990). The LMS method for constructing normalized growth standards. *European Journal of Clinical Nutrition* **44**, 45–60.
- Dosenbach NUF, Nardos B, Cohen AL, Fair DA, Power JD, Church JA, Nelson SM, Wig GS, Vogel AC, Lessov-Schlaggar CN, Barnes KA, Dubis JW, Feczko E, Coalson RS, Pruett JR, Barch DM, Petersen SE, Schlaggar BL** (2010). Prediction of individual brain maturity using fMRI. *Science (New York, N.Y.)* **329**, 1358–1361.
- Fichter M, Quadflieg N** (2001). The structured interview for anorexic and bulimic disorders for DSM-IV and ICD-10 (SIAB-EX): reliability and validity. *European psychiatry: the journal of the Association of European Psychiatrists* **16**, 38–48.
- Fornito A, Zalesky A, Bullmore ET** (2010). Network scaling effects in graph analytic studies of human resting-state FMRI data. *Frontiers in Systems Neuroscience* **4**, 22.
- Geisler D, Borchardt V, Lord AR, Boehm I, Ritschel F, Zwipp J, Clas S, King JA, Wolff-Stephan S, Roessner V, Walter M, Ehrlich S** (2016). Abnormal functional global and local brain connectivity in female patients with anorexia nervosa. *Journal of Psychiatry & Neuroscience : JPN* **41**, 6–15.
- Gollub RL, Shoemaker JM, King MD, White T, Ehrlich S, Sponheim SR, Clark VP, Turner JA, Mueller BA, Magnotta V, O’Leary D, Ho BC, Brauns S, Manoach DS, Seidman L, Bustillo JR, Lauriello J, Bockholt J, Lim KO, Rosen BR, Schulz SC, Calhoun VD, Andreasen NC** (2013). The MCIC collection: a shared repository of multi-modal, multi-site brain image data from a clinical investigation of schizophrenia. *Neuroinformatics* **11**, 367–388.
- Gorgolewski K, Burns CD, Madison C, Clark D, Halchenko YO, Waskom ML, Ghosh SS** (2011). Nipype: a flexible, lightweight and extensible neuroimaging data processing framework in python. *Frontiers in Neuroinformatics* **5**, 13.
- Gunn SR** (1998). Support Vector Machines for Classification and Regression. In *Technical Report* vol 14, pp85–86. School of Electronics and Computer Science: University of Southampton.
- Hagberg AA, Schult DA, Swart PJ** (2008). Exploring network structure, dynamics, and function using NetworkX. In *Proceedings of the 7th Python in Science Conference (SciPy2008)*, pp11–15. Pasadena, CA USA.
- Hagmann P, Cammoun L, Gigandet X, Meuli R, Honey CJ, Wedeen VJ, Sporns O** (2008). Mapping the structural core of human cerebral cortex. *PLoS biology* **6**, e159.

- Harris PA, Taylor R, Thielke R, Payne J, Gonzalez N, Conde JG** (2009). Research electronic data capture (REDCap)--a metadata-driven methodology and workflow process for providing translational research informatics support. *Journal of Biomedical Informatics* **42**, 377–381.
- Hautzinger M, Kühner C, Keller F** (2009). *BDI-II Beck-Depressions-Inventar*. 2nd edn. Pearson Assessment & Information GmbH: Frankfurt.
- Hebebrand J, Casper R, Treasure J, Schweiger U** (2004). The need to revise the diagnostic criteria for anorexia nervosa. *Journal of Neural Transmission (Vienna, Austria: 1996)* **111**, 827–840.
- Hebebrand J, Himmelmann GW, Hesecker H, Schafer H, Remschmidt H** (1996). Use of percentiles for the body mass index in anorexia nervosa: diagnostic, epidemiological, and therapeutic considerations. *The International Journal of Eating Disorders* **19**, 359–369.
- Hemmelmann C, Brose S, Vens M, Hebebrand J, Ziegler A** (2010). Percentiles of body mass index of 18-80-year-old German adults based on data from the Second National Nutrition Survey. *Deutsche Medizinische Wochenschrift (1946)* **135**, 848–852.
- Kromeyer-Hauschild K, Wabitsch M, Kunze D, Geller F, Geiß H, Hesse V, Von Hippel A, Jaeger U, Johnsen D, Korte W, others** (2001). Perzentile für den Body-mass-Index für das Kindes- und Jugendalter unter Heranziehung verschiedener deutscher Stichproben. *Monatsschrift Kinderheilkunde* **149**, 807–818.
- Munkres J** (1957). Algorithms for the Assignment and Transportation Problems. *Journal of the Society for Industrial and Applied Mathematics* **5**, 32–38.
- Newman MEJ** (2002). Assortative Mixing in Networks. *Physical Review Letters* **89**, 208701.
- Ojala M, Garriga GC** (2010). Permutation tests for studying classifier performance. *Journal of Machine Learning Research* **11**, 1833–1863.
- Paul T, Thiel A** (2005). *Eating Disorder Inventory-2 (EDI-2)*. Hogrefe: Göttingen.
- Pedregosa F, Varoquaux G, Gramfort A, Michel V, Thirion B, Grisel O, Blondel M, Prettenhofer P, Weiss R, Dubourg V, others** (2011). Scikit-learn: Machine learning in Python. *Journal of Machine Learning Research* **12**, 2825–2830.
- Petermann F, Petermann U** (2006). *Hamburg Wechsler Intelligenztest für Kinder IV (HAWIK-IV)*. Huber: Bern.
- Power JD, Barnes KA, Snyder AZ, Schlaggar BL, Petersen SE** (2012). Spurious but systematic correlations in functional connectivity MRI networks arise from subject motion. *NeuroImage* **59**, 2142–2154.
- R Core Team** (2012). *R: A Language and Environment for Statistical Computing*. . R Foundation for Statistical Computing: Vienna, Austria
- Saad ZS, Gotts SJ, Murphy K, Chen G, Jo HJ, Martin A, Cox RW** (2012). Trouble at rest: how correlation patterns and group differences become distorted after global signal regression. *Brain Connectivity* **2**, 25–32.
- Schmitz N, Hartkamp N, Kiuse J, Franke GH, Reister G, Tress W** (2000). The Symptom Check-List-90-R (SCL-90-R): a German validation study. *Quality of Life Research: An International Journal of Quality of Life Aspects of Treatment, Care and Rehabilitation* **9**, 185–193.

Yan C-G, Zang Y-F (2010). DPARSF: A MATLAB Toolbox for 'Pipeline' Data Analysis of Resting-State fMRI. *Frontiers in systems neuroscience* **4**, 13.